THE STRUCTURE OF THE IO PLASMA TORUS AFTER ULYSSES ENCOUNTER

N. Meyer-Vernet* and M. Moncuquet*

Abstract

A good knowledge of the Io plasma torus is necessary to interpret Jovian radio-emissions. Before Ulysses encounter, the torus spatial structure was mainly deduced from its crossing by Voyager 1, which took place close to the equator. This gave few observational constraints on the latitudinal structure, which was thus modelled using untested assumptions. Contrary to Voyager and to Galileo, Ulysses crossed the torus basically north-to-south. This allowed the in-board radio experiment to measure *in situ* the latitudinal variation of the electron density and bulk temperature, using quasi-thermal noise analysis. The temperature was found to increase significantly with latitude, which contradicts the isothermal assumption made in the classical torus models. This result can be explained if the bulk velocity distributions have an excesss of particles with energy just above thermal, i.e., are Kappa-like, as often observed in space plasmas. These findings imply an important revision of the torus models and a reinterpretation of some Voyager results.

1 Introduction

The Io plasma torus poses difficult problems involving both aeronomy [Brown et al., 1983] and plasma physics [Hill et al., 1983], as it interacts with the atmosphere of Io – which is the most volcanically active body known, and with Jupiter's magnetosphere – which is largely dominated by rotation. Understanding this object is a perequisite to understand Jovian radioemissions, since a large part of them is believed to come from regions magnetically connected to Io or from the torus itself [Kaiser, 1993]. In addition, the electron density gradients substantially modify wave propagation, so that a reliable density model is needed to calculate wave refraction, diffraction, and dispersion.

Before 1992, most of the knowledge on the torus density and temperature came from the Voyager 1 encounter. However, that spacecraft only explored the vicinity of the torus equator, measuring *in situ* the plasma as a function of Jovicentric distance. Hence, in the two-dimensional torus models, the latitudinal structure could not be based on

*Département de Recherche Spatiale, CNRS, Observatoire de Paris, 92195 Meudon Cedex, FRANCE

in situ measurements but had to be deduced from theory, using plausible but untested assumptions [Bagenal and Sullivan, 1981; Bagenal, 1994]. Galileo could not solve this problem either, since it also crossed the torus near the equator. On the contrary, Ulysses made a basically north-to-south traversal, exploring the torus over several scale heights in vertical distance on both sides of the equator, with a small variation in radial distance and longitude (Figure 1). Most importantly, a large part of this trajectory followed a magnetic shell near $L \approx 8$.

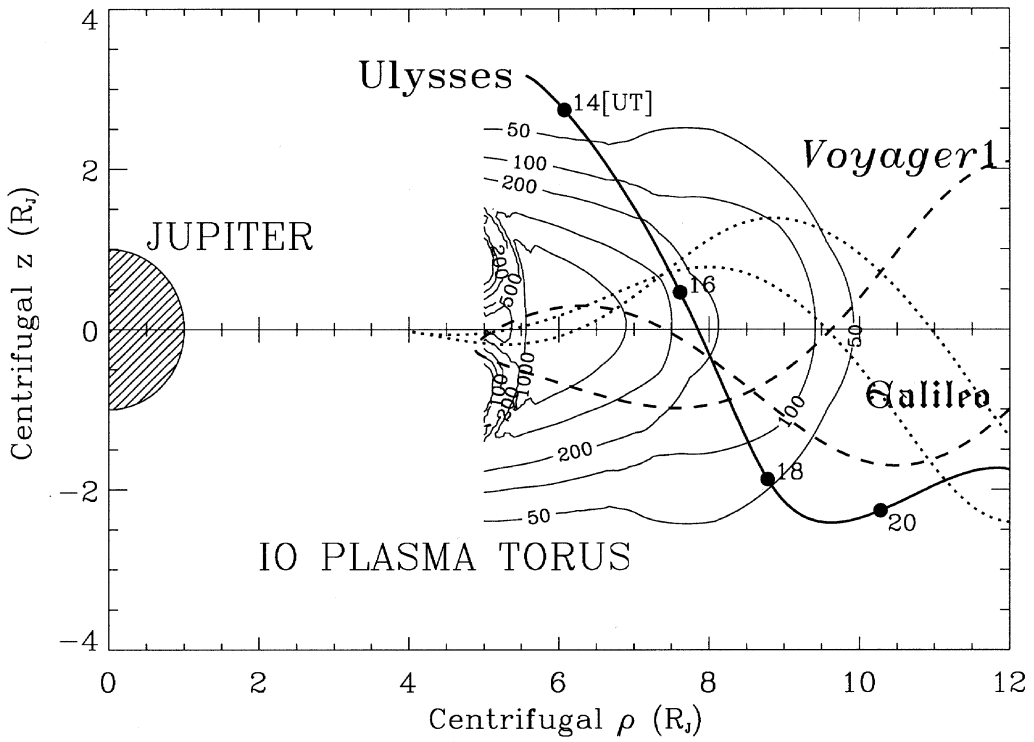

Figure 1: Passages of Ulysses (heavy line), Voyager 1 (dashed), and Galileo (dotted) in the Io plasma torus. The trajectories are shown in cylindrical coordinates, ρ, parallel to the centrifugal equator, and z, perpendicular. The time (in hours) is plotted along Ulysses trajectory. The light lines are isodensity contours adapted from Bagenal [1994].

The particle analyzers were not operating in this region, but the radio experiment URAP [Stone et al., 1992a] measured *in situ* the electron density and temperature, from quasi-thermal noise analysis [Meyer-Vernet et al., 1993; Hoang et al., 1993; Moncuquet et al., 1995]. This performance was made possible by three properties of the URAP instrument: (1) the radio receiver is one of the most sensitive ever flown, (2) the length of the spin plane electric antenna was of the order of magnitude of the thermal electron gyroradius, making it well adapted to measure quasi-thermal Bernstein waves, and (3) the spacecraft spin modulation produced a large variation of the antenna orientation with respect to the ambient magnetic field, thus allowing to measure the wave vector. The results obtained contradict the isothermal assumption made in the classical torus models, thus yielding an important revision of these models.

2 Using a radio experiment to measure the electron density and temperature and the magnetic field

The upper panel of Figure 2 (color plate) is a radio spectrogram acquired by the URAP radio receivers during the torus crossing, and farther out from Jupiter. We have superimposed the plasma frequency, as deduced from the enhanced noise near the upper-hybrid frequency f_{UH}, in the dense region where $f_{UH} \gg f_g$, the electron gyrofrequency; we have also drawn a few harmonics of f_g, and the first Bernstein f_Q frequency. The lower panel shows the electron density and temperature, and the magnetic field modulus deduced from this spectrogram by different methods [Meyer-Vernet et al., 1993; Hoang et al., 1993; Moncuquet et al., 1995; Moncuquet et al., 1997].

Apart from the upper-hybrid noise and a few bursty emissions, the most conspicuous features of this spectrum are smooth banded noise between consecutive gyroharmonics, below the plasma frequency. Figure 3 shows the minima and maxima of the signal in these bands as a function of time. One sees that the level is very stable, except within a few degrees of the magnetic equator. The minima take place at gyroharmonics, and their detection gives the modulus of the ambient magnetic field, with an accuracy of a few percent [Meyer-Vernet et al., 1993], as compared to the in-board magnetometer. It is important to note that this use of a radio experiment to serve as a magnetometer was made possible by the extreme sensitivity of the URAP receiver, which is about 60 times better than on Voyager and 20 times better than on Galileo in this frequency range (in power units), and by its good frequency resolution.

The maxima take place near the middle of the harmonic bands, and their amplitude is close to the level of the plasma quasi-thermal noise in Bernstein waves, which can be easily estimated with an electron velocity distribution made of a cold (c) plus a hot (h) Maxwellian (the cold population being dominant), of respective temperatures T_c, T_h, as modelled from Voyager data [Sittler and Strobel, 1987].

Bernstein modes are sustained by the electron gyration in the ambient magnetic field $\mathbf{B}$, and propagate without damping perpendicular to $\mathbf{B}$, between the gyroharmonics. The wave number is mainly determined by the gyroradius of the main (cold) electron population, $\rho_c = v_c/\omega_g$, with $v_c = (k_B T_c/m_e)^{1/2}$ and $\omega_g = eB/m_e$; in the middle of the gyroharmonic bands, it is of order $k_\perp \sim 1/\rho_c$. The noise at the mid-band maxima is produced by the hot electrons, and correspond to waves having a sufficiently small parallel wave number $k_\parallel$ for the damping by the main cold electron population to be negligible, which requires $k_\parallel v_c$ to be sufficiently small compared to $\omega - n\omega_g$, (n being the order of the harmonic band considered), i.e., $\left|k_\parallel\right| \leq \Delta k_\parallel \sim 0.1/\rho_c \ll k_\perp$. Note that this spread in $k_\parallel$ (which defines the wave vectors for which the noise is produced by the hot electrons) vanishes at gyroharmonics, where the noise has minima; at these minima, the noise is then produced by the (main) cold population.

The mean electrostatic energy of the quasi-thermal fluctuations per unit volume at the mid-band maxima is

$$\epsilon_0 \left\langle E^2 \right\rangle /2 \;\; \sim \;\; \mathcal{N} k_B T_h \tag{1}$$

Here E is the electrostatic field, and $\mathcal{N}$ the number of modes $\mathbf{k}$ per unit volume, i.e., $\mathcal{N} = \mathcal{V}/(2\pi)^3$, where $\mathcal{V}$ is the volume occupied in $\mathbf{k}$ space by the relevant modes. Approximating this volume by a cylinder of radius $k_\perp$ and small width $2\Delta k_\parallel$ with values estimated above, we find $\mathcal{V} \sim 0.2\pi/\rho_c^3$. Substituting in (1), and noting that the bandwidth is of order f_g, we deduce the electric field power spectral density at the maxima

$$E_\omega^2 \sim \left\langle E^2 \right\rangle / f_g \sim \frac{0.1 k_B T_h}{\pi \epsilon_0 \omega_g \rho_c^3} \quad (2)$$

For a short antenna making an angle θ with $\mathbf{B}$, i.e., with $L \sin\theta < \rho_c$, the voltage power spectral density is $V_\omega^2 \sim E_\omega^2 L^2 \sin^2\theta$. A more rigorous calculation [Sentman, 1982] yields roughly the same result for a short antenna. Putting for Ulysses $L = 35$ m, and typical plasma parameters at 15:30 UT for example: $T_c \sim 2 \times 10^5$ K, $T_h \sim 10^7$ K, $f_g \sim 26$ kHz, we find: $V_\omega^2 \sim 4 \times 10^{-12}$ $\mathrm{V^2 Hz^{-1}}$. This is roughly the level observed at this time (see Figure 3).

Hence, these noise bands are not produced by plasma instabilities. Contrary to what has often been claimed, the same is generally true of similar "$(n + 1/2)\, f_g$" noise bands observed in other magnetospheres; this is also true of the bands observed in the same region by Birmingham et al. [1981], as was first suggested by Couturier et al. [1981], and verified by Sentman [1982].

For a large part of the data, the antenna is not small compared to the thermal gyroradius, so that the antenna response, and thus the variation of the noise with the antenna orientation is different. We have plotted in the upper panel of Figure 4 a typical spectrum in the torus, showing the first gyroharmonic band and the beginning of the second one, with the minima at gyroharmonics. The small-scale modulation is due to the spacecraft spin during a frequency sweep, which changes periodically the angle θ between the antenna and the magnetic field $\mathbf{B}$, as shown at the top of the figure. One sees that in the high-frequency part of the gyroharmonic band, the signal has a maximum when the antenna is perpendicular to $\mathbf{B}$. This is not surprising, since for Bernstein waves k is small in the high-frequency part of the bands, so that the antenna is very short compared to the wavelength; hence the antenna response for electrostatic waves ($\mathbf{E} \parallel \mathbf{k}$) has a maximum when it is parallel to $\mathbf{k}$, and thus perpendicular to $\mathbf{B}$. On the other hand one sees that in the middle of the harmonic band, V_ω^2 has a plateau at $\theta = \pi/2$, whereas in the low-frequency part of the band, V_ω^2 has a minimum at $\theta = \pi/2$. Again, this is not surprising since for Bernstein waves k becomes very large in the low-frequency part of the bands, so that the antenna is no longer short.

Basically, a dipole antenna made of two thin wires – each of length L, mainly "sees" the

Figure 2: (plate, next page) Upper panel: Radio spectrogram measured by URAP on Ulysses in the Io plasma torus and beyond, displayed as frequency versus time, with intensity coding indicated by the bar chart on the right. We have superimposed the plasma frequency f_p, a few electron gyroharmonics, and the first f_Q Bernstein frequency. Lower panel: Corresponding electron density, bulk temperature, and magnetic field deduced from quasi-thermal noise analysis, as a function of time, Jovicentric distance, and magnetic latitude (top scale of the upper panel).

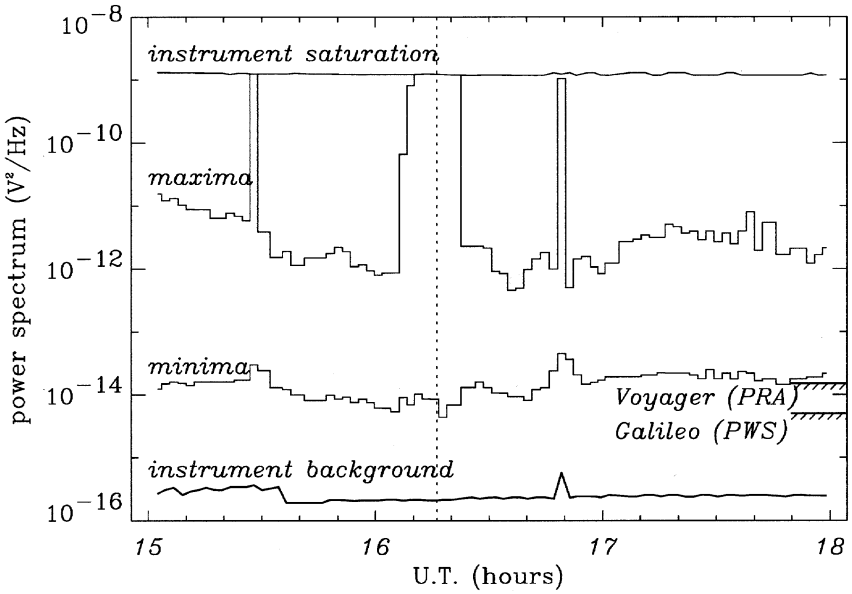

Figure 3: Minima and maxima (from the gyrofrequency to 48 kHz) for the URAP spectra acquired during the torus crossing. The top and bottom curves show respectively the instrument noise level at the frequency of each minimum, and the instrument saturation level. We have indicated for comparison the instrumental noise levels of PRA aboard Voyager, and of PWS aboard Galileo. The vertical dotted line indicates the magnetic equator crossing .(Adapted from Moncuquet et al. [1995]).

electrostatic waves whose half projected wavelength equals L. To yield $k_{projected}L \approx \pi$ with $kL \gg 1$, $\mathbf{k}$ must be roughly perpendicular to the antenna [Meyer-Vernet and Perche, 1989]; (see a picture of the electrostatic angular response in Meyer-Vernet, [1994]).

More precisely, it can be shown that the Bernstein wave power at the antenna ports varies with the angle θ between the antenna and $\mathbf{B}$ as $V_\omega^2 \propto F_\perp(kL\sin\theta)$, with

$$F_\perp(u) = \frac{64}{\pi}\int_0^u dt \frac{\sin^4(t/2)}{t^2(u^2-t^2)^{1/2}} \tag{3}$$

The corresponding theoretical spin modulation is plotted in Figure 5 for three values of kL. (Recall that $k \approx k_\perp$). It reproduces the behavior observed, i.e., a $\sin^2\theta$ variation for a short antenna (since $F_\perp(u) \approx u^2$ for $u \leq 1$), a plateau for $kL \sim 3$, and a minimum at $\theta = \pi/2$ for a long antenna [Meyer-Vernet et al., 1993].

This has an important consequence. Provided the antenna length L is of the order of half the wavelength or longer, one can deduce k by fitting the theoretical spin modulation to the data. Doing that for a set of frequencies yields the wave dispersion curve. An example is given in the bottom panel of Figure 4, which shows the dispersion curve deduced from the data in the top panel [Moncuquet et al., 1995]. The Bernstein dispersion curves only depend on the magnetic field, and on the electron density and temperature. Since the two first parameters are known, the temperature can be deduced by fitting the theoretical Bernstein curve to the measured dispersion curve [Meyer-Vernet et al., 1993; Moncuquet

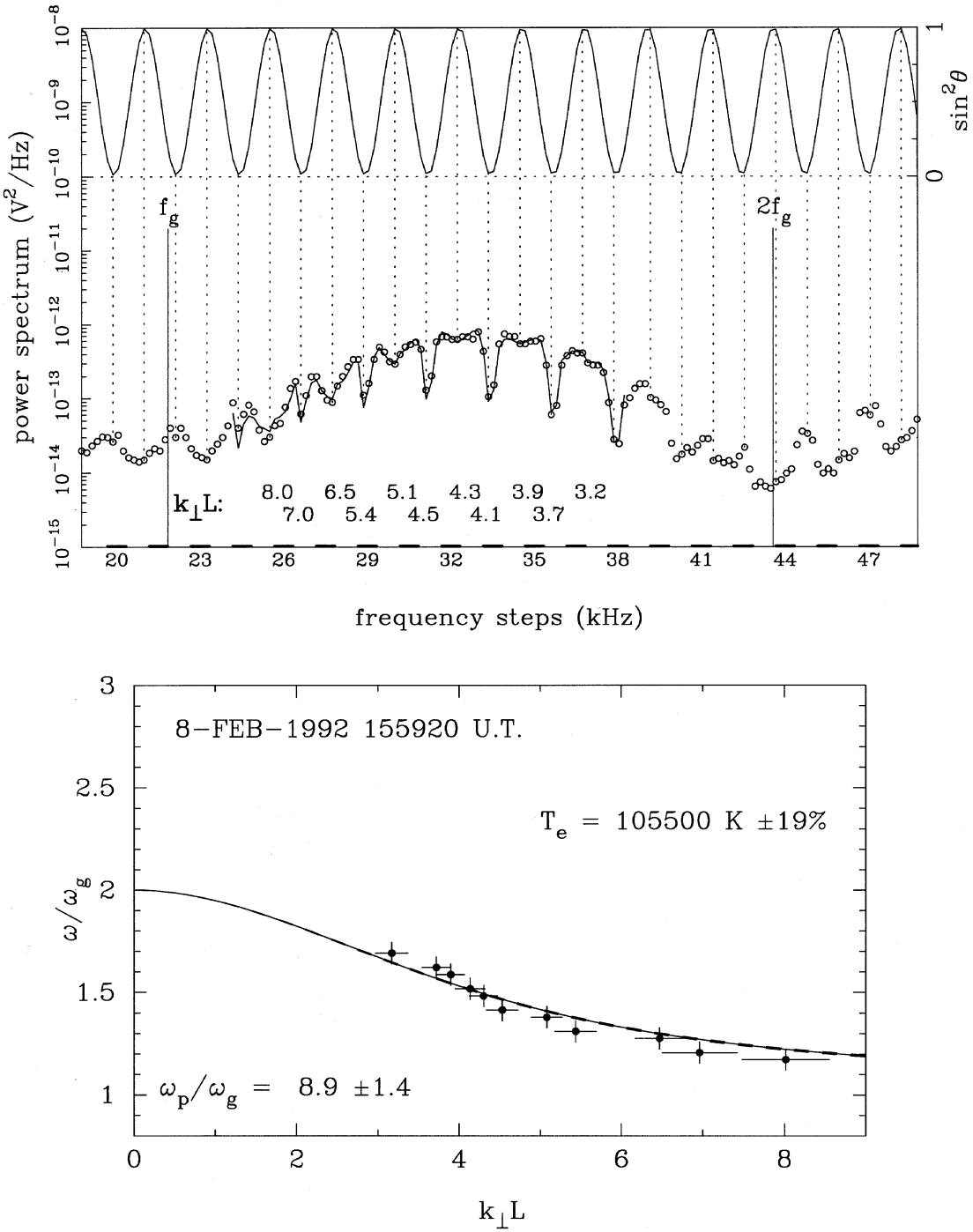

Figure 4: Upper panel: A typical URAP spectrum acquired on Ulysses in the torus (15:59:20 UT on February 8, 1992) in the first gyroharmonic band and the beginning of the second one. The small circles are the measurements and the solid line is the best-fit antenna response, with the deduced values of kL indicated just below. The angle θ between the antenna and the magnetic field is plotted at the top. Lower panel: Corresponding dispersion curve. The points with errors bars are deduced from the observed spectrum, and the solid line is the best-fitted solution of Bernstein dispersion equation with the corresponding (bulk) electron temperature indicated (Adapted from Moncuquet et al. [1995]).

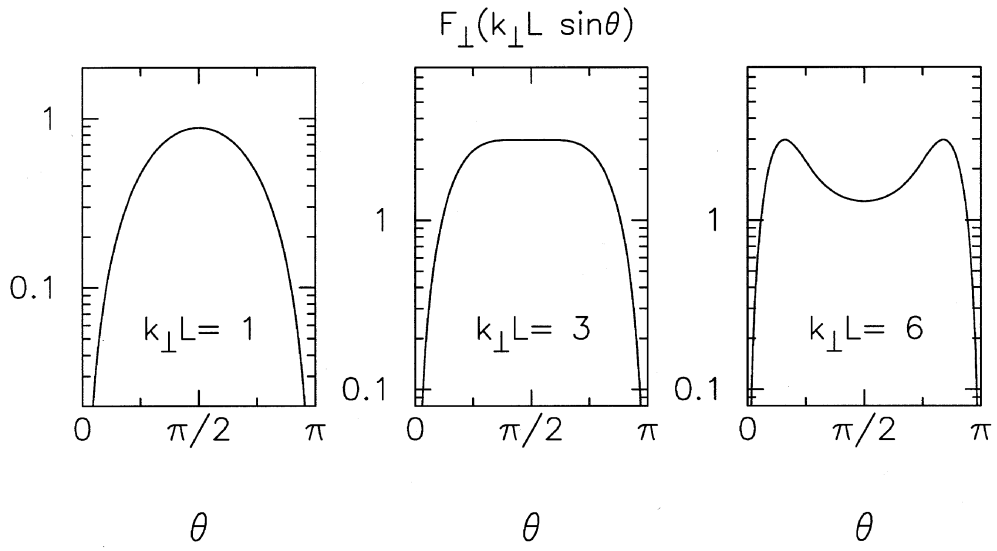

Figure 5: Antenna response for Bernstein waves, $F_\perp\,(kL\sin\theta)$, plotted versus the angle θ between the antenna and the magnetic field for three values of kL ($k \approx k_\perp$). The predicted spin modulation varies as $\sin^2\theta$ for $kL \leq 1$, but has a minimum at $\theta = \pi/2$ for $kL > 3$. (Adapted from Meyer-Vernet et al. [1993]).

et al., 1995]. Since that temperature is the sole unknown parameter, its determination can be rather precise.

Note that since the antenna is not short at the midband maxima, the quasi-thermal noise V_ω^2 estimated above must be corrected by taking the actual antenna response into account, namely by replacing $V_\omega^2 = E_\omega^2 L^2$ by $V_\omega^2 = E_\omega^2 F_\perp\,(kL\sin\theta)\,/k^2$. Substituting the maximum value $F_\perp = 3$ (see Figure 5), and E_ω^2 given in Equation (2), we get the following corrected estimate for the amplitude at the midband maxima

$$V_\omega^2 \;\sim\; \frac{0.3 k_B T_h}{\pi \epsilon_0 v_c} \tag{4}$$

for $L \geq \rho_c = v_c/\omega_c$, with $v_c = (k_B T_c/m_e)^{1/2}$. In practical units, this yields

$$V_\omega^2 \;\sim\; 4 \times 10^{-17} T_h/\sqrt{T_c} \quad \mathrm{V^2 Hz^{-1}} \tag{5}$$

with T_c, T_h in ^{o}K. (Note that this does not change the order of magnitude calculated at the beginning of this section).

3 Implications of the temperature measurements

As already noted, the electron distribution measured by the Voyager particle analyzers was modelled by a superposition of two Maxwellians, with the hot population 10–30 times hotter than the cold population, and representing a few percent of the total density. The actual distribution is in fact more complex, since the hot electrons were clearly not

Maxwellian distributed [Scudder et al., 1981]. Furthermore, a significant part of the main (cold) population could not be detected, owing to the 10-eV instrumental threshold, (and to the negative spacecraft potential).

With such a non-Maxwellian distribution, with the cold population being dominant and not too far from a Maxwellian, it can be shown that the Ulysses temperature determination based on Bernstein dispersion characteristics yields an effective temperature which is defined from the mean *inverse* energy of the particles [Moncuquet et al., 1995]. It is thus mainly sensitive to the cold electrons; in fact, it involves just the same mean as in the classical Debye shielding, albeit for different reasons [Meyer-Vernet, 1993]. For a sum of two Maxwellians, this effective temperature T_{eff} is given by

$$1/T_{eff} \quad = \quad (n_c/T_c + n_h/T_h) \,/\, (n_c + n_h) \tag{6}$$

instead of the classical temperature $T = (n_c T_c + n_h T_h) \,/\, (n_c + n_h)$, which is defined from the mean energy. With the parameters measured by Voyager, $T_{eff} \approx T_c$.

Figure 6 shows this measured temperature versus the electron density, with the associated best-fit line. This yields the polytrope relation

$$T_{eff} \quad \propto \quad n^{\gamma-1} \tag{7}$$

with $\gamma = 0.48 \pm 0.06$ (3 σ). The correlation coefficient is $r = -0.87$. Given the number of data points (46), the level of significance of this anticorrelation is very high.

Note that the geometry of the Ulysses trajectory, and the general predominance of the latitudinal gradient over the radial one, ensure that most of the variation observed here in density and temperature can be ascribed to the change in latitude. Note also that the electron free paths are much larger than the latitudinal scale height ($\sim 1 R_J$), so that the time for a particle to move over a characteristic scale length along $\mathbf{B}$ is short compared to collisional time scales.

The polytrope relation $T_{eff} \propto 1/\sqrt{n}$ (with $T_{eff} \approx T_c$) found here over more than a decade is clearly incompatible with the torus models, which assume diffusive equilibrium along $\mathbf{B}$ with *constant temperature for each population*, to extrapolate outside equator the density measured *in situ* by Voyager [Bagenal and Sullivan, 1981; Bagenal, 1994].

The main external force acting on the charged particles along $\mathbf{B}$ is produced by the centrifugal force due to the plasma corotation. Since the electrons are much lighter than ions, they feel a much smaller centrifugal force, so that an ambipolar electric field must exist to preserve local charge quasi-neutrality. This field confines the electrons in the same region as ions, i.e. near the point along any given magnetic field line where the $\mathbf{B}$-aligned component of the centrifugal force vanishes [Gledhill, 1967]; this defines the so-called centrifugal equator (which is slightly shifted from the magnetic equator since the planet's magnetic and spin axis do not exactly coincide).

In a first approximation, the particles are thus confined near the equator by forces deriving from potentials: the electrostatic force for electrons, the electrostatic force plus the centrifugal one for ions. Let Φ be the total potential acting on a given species (we do not consider very high latitudes, so that Φ increases in a monotonic way along $\mathbf{B}$, starting

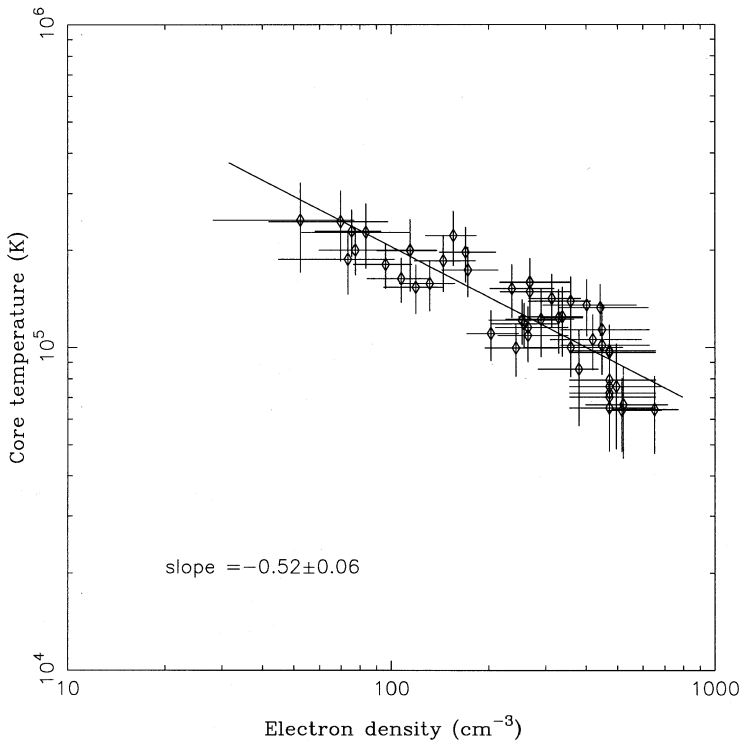

Figure 6: Electron density and bulk temperature measured in situ *aboard Ulysses, and the associated best-fit line. The data span* $\sim 3R_J$ *along field lines. (The longitude varies by* $\approx 90^o$*, centered near* 310^o *CML, and the Jovicentric distance only varies from 7.1 to 8.4* R_J*). (From Meyer-Vernet et al. [1995]).*

from the equator). In the classical torus models, which use a fluid description with a constant temperature for each species, the density of a species of temperature T varies along $\mathbf{B}$ as the Boltzmann factor, $n \propto \exp(-\Phi/k_B T)$. Equivalently, one can use instead microscopic equations, (i.e., take the particle velocity distributions into account and use Liouville theorem), and *assume Maxwellian distributions* at the equator. In that case, one finds that the temperatures again do not vary along $\mathbf{B}$, and that the densities again follow the Boltzmann law. (Note that with anisotropic Maxwellians, the perpendicular temperatures would change along $\mathbf{B}$, owing to the mirror force [Huang and Birmingham, 1992], but this effect is negligible for electrons, since (1) their anisotropy is expected to be small [Sittler and Strobel, 1987], and (2) the magnetic field modulus does not change very much in the latitude range considered.)

This clearly shows that the classical torus description must be changed in a basic way. First, owing to the large free paths, one must use microscopic equations. Second, one must consider non-Maxwellian distributions for each species, since Maxwellians would produce constant temperatures along field lines.

4 Velocity filtration in the Io torus and Kappa distributions

To calculate the density variation along field lines, we have to find how particles having a non-Maxwellian velocity distribution are spatially distributed in an attracting potential. This problem is similar to the altitude stratification of a dilute atmosphere confined by gravity, and has been studied by Scudder [1992a,b] in a different context, to interpret temperature inversions in stellar coronae. Basically, since the more energetic particles overcome more easily the confining potential, their proportion is larger outside the potential well, so that the mean kinetic energy of particles increases with latitude as the density falls. This does not happen with a Maxwellian distribution because in that case the potential filtrates all the particles in the same way (it produces a translation in energy which reduces to a multiplicative factor, since $e^{-E-\Phi} = e^{-E} \times e^{-\Phi}$).

This velocity filtration effect is best illustrated in the simple situation when the velocity distribution at equator (where the potential is taken to be zero) is a sum of two Maxwellians of densities n_c, n_h, and temperatures T_c, T_h, respectively. Let us assume $n_h \ll n_c$ and $n_h T_h \ll n_c T_c$, so that the temperature at equator is $T(0) = (n_c T_c + n_h T_h)/(n_c + n_h) \approx T_c$. Let us now calculate the temperature at the position s where the potential is Φ, when $k_B T_c \ll \Phi \ll k_B T_h$. The cold and hot densities vary as

$$n_c(s) = n_c e^{-\Phi/k_B T_c} \quad (8)$$

$$n_h(s) = n_h e^{-\Phi/k_B T_h} \quad (9)$$

From the above inequalities, we have $n_c(s) \approx 0$ and $n_h(s) \approx n_h$, so that the temperature is now: $T(s) \approx T_h$. Hence the temperature has increased with altitude, whereas the total density has decreased. This also holds when the temperature is defined from the mean inverse energy as in Equ. (6), namely for the temperature T_{eff}. These results can be generalized to any distribution made of a sum of Maxwellians in a monotonic attracting potential [Meyer-Vernet et al., 1995].

A more convenient model for a non-Maxwellian distribution is the "Kappa" distribution

$$f(v) \propto \left[1 + \frac{v^2}{\kappa V^2}\right]^{-\kappa-1} \quad (10)$$

It is very useful to model observed velocity distributions (see, for example, Vasyliunas, [1968]; Kane et al., [1992]) since it is quasi-Maxwellian at low and thermal energies, whereas its non-thermal tail decreases as a power-law at high energies, as generally observed in space plasmas; this is in line with the fact that particles of higher energy have larger free paths, and are thus less likely to achieve partial Maxwellian equilibrium [Scudder, 1992a]. For typical space plasmas, κ generally lies in the range 2–6.

This Kappa distribution tends to a Maxwellian for $\kappa \to \infty$ since

$$\lim_{\kappa\to\infty} \left[1 + \frac{v^2}{\kappa V^2}\right]^{-\kappa-1} = \exp\left(-v^2/V^2\right) \quad (11)$$

Consider now a Kappa velocity distribution $f_0(v)$ at altitude 0. The distribution at altitude s, where the potential is Φ, is given from Liouville theorem by $f(s,v) = f_0(v_0)$

with $v^2 = v_0^2 - 2\Phi/m$, from conservation of energy. With a monotonic attracting potential, all the phase space trajectories at s connect to $s = 0$, and it can then be easily shown that the density $n(s) = \int d^3v f(s, v)$ and the temperature T are given by [Scudder, 1992a]

$$\frac{n(s)}{n(0)} = \left[1 + \frac{2\Phi}{\kappa m V^2}\right]^{-\kappa+1/2} \tag{12}$$

$$T \propto n^{\gamma-1} \quad \text{with} \quad \gamma = 1 - \frac{1}{\kappa - 1/2}. \tag{13}$$

Hence, with a Kappa velocity distribution in an attracting potential Φ, the density varies with Φ like a Kappa function (instead of a Gaussian), and the temperature follows a polytrope law of index $\gamma < 1$. It can be shown that the same polytrope law holds when the temperature is defined from the mean inverse energy, i.e., for the temperature T_{eff} measured by Ulysses.

Note that in the limit $\kappa \to \infty$, i.e., a Maxwellian velocity distribution, Equ. (13) yields $\gamma \to 1$, i.e., the temperature is a constant, which is the classical result for a Maxwellian. Note also that the density profile (12) can be deduced equivalently using fluid equations with the polytrope law (13) [Meyer-Vernet et al., 1995].

From the polytrope law found by Ulysses with $\gamma = 0.48$, we deduce from Equ. (13)

$$\kappa \approx 2.4 \pm 0.2 \tag{14}$$

for electrons. Figure 7 compares this Kappa function with a sum of two Maxwellians having parameters of the order of those inferred from Voyager analyzers in the range of Jovicentric distances explored here [Sittler and Strobel, 1987; Bagenal, 1994].

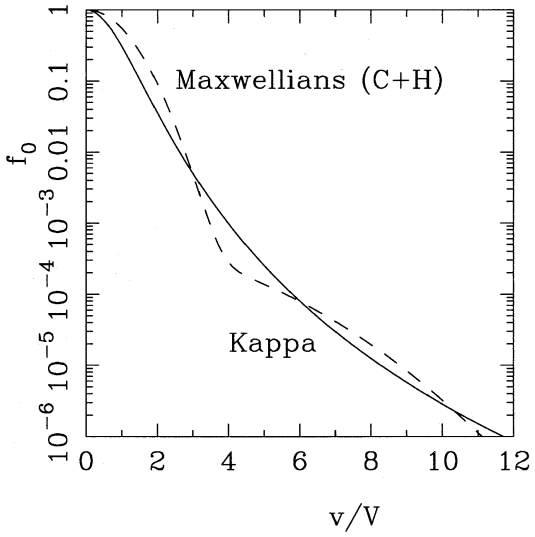

Figure 7: Kappa distribution (with $\kappa = 2.4$ as deduced from URAP measurements for the electrons) compared with a sum of a cold (c) and a hot (h) Maxwellian of densities and temperatures satisfying $n_h/n_c = 0.02$, $T_h/T_c = 12$. (Adapted from Meyer-Vernet et al., [1995]).

5 Towards a new model of the Io torus

The above results have important implications for the torus models, since they suggest that the usual Gaussian profiles must be replaced by Kappa-like profiles. These Ulysses results concern only the electrons, and the ion velocity distributions were not measured. They could not be unambiguously determined from Voyager measurements either, because the spectra of individual species could not be resolved; anyway, the data indicated that the ion velocity distributions were not Maxwellian in the corotating frame [Bagenal and Sullivan, 1981], as suggested by the theoretical models [Smith and Strobel, 1985].

Hence, it is reasonable to model also the ion distributions by Kappa functions. We then calculate the plasma density profile by using profiles of the form Equ. (12) for each species, with the potential $\Phi_e \approx -e\phi_E$ for electrons and $\Phi_i = Ze\phi_E + \phi_C$ for ions of charge Ze, ϕ_C being the centrifugal potential, and ϕ_E the electrostatic potential, which is deduced from local charge neutrality. We have drawn in Figure 8 the resulting plasma density profile when the electron Kappa, κ_e is given in Equ. (14), and the ion mass is $m_i = 20\, m_p$ with $Z = 1$, for two different values of κ_i, compared to the Maxwellian case ($\kappa_i \to \infty$). One sees that the Kappa-like profiles are more confined than the Gaussian near the equator, but less confined farther out.

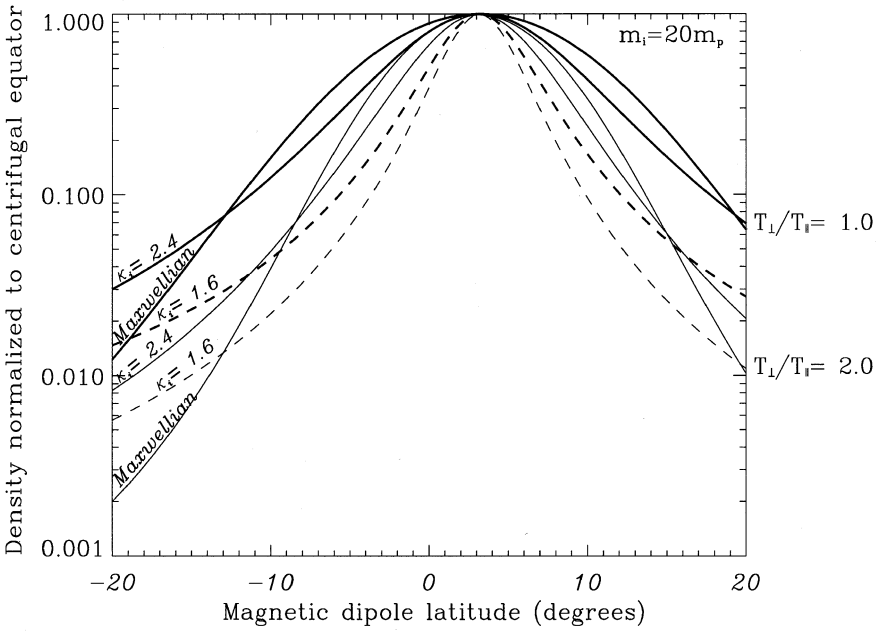

Figure 8: Plasma density (normalized to the value at centrifugal equator) versus magnetic dipole latitude, for two values of the ion Kappa, κ_i, compared to the profile corresponding to Maxwellian ions ($\kappa_i \to \infty$), for ions of mass $m_i = 20m_p$ and charge e. The profiles obtained with isotropic distributions are plotted as heavy lines. We have superimposed as thin lines the profiles obtained with an ion temperature anisotropy $T_\perp/T_\parallel = 2$. (From Moncuquet [1997]).

Since the ion velocity distributions are expected to have a significant anisotropy, we have generalized the model to this case. The ion velocity distribution at $s = 0$ has then the

form

$$f_i(v) \propto \left[1 + \frac{v_\parallel^2}{\kappa_i V_{i\parallel}^2} + \frac{v_\perp^2}{\kappa_i V_{i\perp}^2}\right]^{-\kappa_i - 1} \tag{15}$$

instead of Equ. (10), with the temperature anisotropy factor $A(0) = V_{i\perp}^2/V_{i\parallel}^2 = T_{i\perp}(0)/T_{i\parallel}(0)$. Applying Liouville theorem with conservation of energy and magnetic moment $\mu \propto v_\perp^2/B$, yields the ion density and temperature profiles

$$\frac{n_i(s)}{n_i(0)} = \left[1 + \frac{2\Phi_i}{\kappa_i m_i V_{i\parallel}^2}\right]^{-\kappa_i + 1/2} \frac{A(s)}{A(0)} \tag{16}$$

$$T_{i\parallel} \propto n_i^{\gamma_i - 1} \quad \text{and} \quad 1/A(s) - 1 = [1/A(0) - 1]\, B(0)/B(s) \tag{17}$$

where $\gamma_i = 1 - 1/(\kappa_i - 1/2)$ as in Equ. (13) and $A(s) = T_{i\perp}(s)/T_{i\parallel}(s)$ is the anisotropy factor at position s. In the limit $\kappa_i \to \infty$ (bi-Maxwellian), this reduces to the result by Huang and Birmingham [1992]; in the limit $A(0) = 1$ (isotropy), this reduces to a profile similar to Equ. (12). The resulting plasma density variation for the case $A(0) = 2$ is superimposed in Figure 8.

6 Final remarks

The geometry of the Ulysses encounter, and the performances of the URAP instrument have provided new constraints on the 2-D models of the Io torus, showing that one must relax the usual assumptions of Maxwellian species, and/or, equivalently, of constant temperatures along field lines.

This opens the way to a new generation of models, in which Ulysses provides the latitudinal structure (and a part of the radial profile), whereas most of the radial structure is deduced from Voyager and Galileo measurements. The weakness of these 2-D models based on spacecraft encounters is that that they neglect the longitudinal and temporal variations [Thomas, 1993], which are more conveniently studied by long-term measurements.

Acknowledgements: We are grateful to our colleague Sang Hoang for providing outstanding Ulysses data which made this work possible, and to Fran Bagenal for numerous discussions.